Delayed Contrast Enhancement and Perfusable Tissue Index in Hypertrophic Cardiomyopathy: Comparison Between Cardiac MRI and PET

Paul Knaapen, MD[1]; Willem G. van Dockum, MD[1]; Olga Bondarenko, MD[1]; Wouter E.M. Kok, MD, PhD[1]; Marco J.W. Götte, MD, PhD[1]; Ronald Boellaard, PhD[2]; Aernout M. Beek, MD[1]; Cees A. Visser, MD, PhD[1]; Albert C. van Rossum, MD, PhD[1]; Adriaan A. Lammertsma, PhD[2]; and Frans C. Visser, MD, PhD[1]

[1]Department of Cardiology, VU University Medical Center, Amsterdam, The Netherlands; and [2]Department of Nuclear Medicine and PET Research, VU University Medical Center, Amsterdam, The Netherlands

Delayed contrast enhancement (DCE) visualized by cardiac MRI (CMR) is a common feature in patients with hypertrophic cardiomyopathy (HCM), presumed to be related to myocardial fibrosis. The pathophysiologic basis of hyperenhancement in this patient group, however, remains unclear as limited histologic comparisons are available. The present study compares the perfusable tissue index (PTI), an alternative marker of myocardial fibrosis obtained by PET, with DCE-CMR in HCM. **Methods:** Twenty-one patients with asymmetric septal HCM, 12 chronic myocardial infarction (MI) patients, and 6 age-matched healthy control subjects were studied with DCE-CMR and PET. PET was performed using ^{15}O-labeled water and carbon monoxide to obtain the PTI. **Results:** No hyperenhancement was observed in control subjects and the PTI was within normal limits (1.10 ± 0.07 [mean ± SD]). In MI patients, the extent of hyperenhancement (25% ± 16% [mean ± SD]) was inversely related to the decrease in the PTI (0.94 ± 0.12; $r = -0.65$, $P < 0.05$). Average hyperenhancement in HCM was 14% ± 12%, predominantly located in the interventricular septum. The PTI in the hypertrophied interventricular septum, however, was not reduced (1.12 ± 0.13). Furthermore, in contrast to MI patients, there was a modest positive correlation between the extent of DCE and the PTI in HCM ($r = 0.45$, $P < 0.05$). **Conclusion:** DCE in the hypertrophied septum of HCM patients is not accompanied by a decline in the PTI, and there is a positive correlation between the extent of DCE and the PTI. These results suggest that hyperenhancement may not be caused solely by fibrotic replacement scarring in this patient group. Other pathologic changes associated with HCM may also cause gadolinium-diethylenetriaminepentaacetic acid hyperenhancement.

Key Words: hypertrophic cardiomyopathy; MRI; delayed contrast enhancement; PET; perfusable tissue index

J Nucl Med 2005; 46:923–929

Received Nov. 16, 2004; revision accepted Feb. 14, 2005.

For correspondence or reprints contact: Paul Knaapen, MD, Department of Cardiology, 6D 120, VU University Medical Center, De Boelelaan 1117, 1081 HV Amsterdam, The Netherlands.

E-mail: p.knaapen@vumc.nl

Hypertrophic cardiomyopathy (HCM) is a relatively common primary cardiac disease with great diversity of morphologic, functional, and clinical features (*1*). Although HCM is associated with a variety of mutations in genes encoding proteins of the sarcomere, connective tissue elements are also involved in the disease process (*2*). Several types of myocardial fibrosis (interstitial, perivascular, replacement, and plexiform) can be found in patients with HCM (*2–13*).

Among several factors, the severity of myocardial fibrosis is of prognostic significance in HCM (*2,5,9,11*). For the purpose of risk stratification, noninvasive assessment of fibrosis is desirable. Gadolinium delayed contrast-enhanced (DCE) cardiac MRI (CMR) allows visualization of fibrotic tissue in patients with coronary artery disease (CAD) (*14,15*). Furthermore, hyperenhancement visualized by DCE-CMR is a common feature of HCM, the extent of which is related to left ventricular function parameters, progressive disease, and markers of clinical risk for sudden death (*16,17*). Although the histologic basis of hyperenhancement in HCM remains unclear as histopathologic comparison is limited to a single case report (*18*), it has been suggested that it most likely represents scar tissue (*16–18*).

The perfusable tissue index (PTI), obtained with PET using ^{15}O-labeled water ($H_2{}^{15}O$) and carbon monoxide ($C^{15}O$), reflects the fraction of the myocardium that is able to exchange water rapidly—that is, is perfusable by water (*19–21*). Differentiation between fibrosis and myocardium can be made on the basis of this principle, and it has been shown that a reduction of the PTI correlates with the extent of fibrosis after infarction (*19*). Furthermore, the PTI is reduced in patients with an advanced stage of idiopathic dilated cardiomyopathy, possibly due to increased interstitial and perivascular fibrosis (*22*). Matched measurements of DCE and PTI can therefore provide more insight into the pathophysiologic nature of DCE in HCM.

The present study was conducted to test whether (a) the PTI is reduced in patients with HCM as compared with

healthy control subjects and (b) the extent to which DCE-CMR and the PTI are related in HCM. As changes in both DCE-CMR and the PTI are well documented in patients with chronic myocardial infarction (MI) (*14,15,19–21*), this patient group served as a reference.

MATERIALS AND METHODS

Patient Population

Twenty-one HCM patients, 12 chronic MI patients, and 6 age-matched healthy volunteers were studied with CMR and PET. HCM was diagnosed by the presence of a nondilated and hypertrophied left ventricle (LV) on 2-dimensional (2D) echocardiography (maximal wall thickness >15 mm in adult index patients or >13 mm in adult relatives of an HCM patient) in the absence of any other systemic or cardiac disease. Exclusion criteria were any absolute or relative contraindication to CMR or PET (e.g., pacemaker, claustrophobia), atrial fibrillation, and history of CAD. All HCM patients had asymmetric septal hypertrophy. CAD was excluded by angiography in 8 patients. Of the remaining 13 patients, 1 had anginal symptoms. CAD was excluded in this particular patient by a negative nuclear imaging stress test. MI was defined by a previously documented typical MI. MI patients with a recent (<1 mo) acute coronary syndrome were excluded. All healthy control subjects underwent physical examination, electrocardiography, and echocardiography. None of the results from these examinations showed any abnormalities. All subjects gave written informed consent, and the protocol was approved by the Medical Ethics Committee of the VU University Medical Center.

Imaging Protocols

PET. All scans were performed in 2D mode, using an ECAT EXACT HR+ scanner (Siemens/CTI). The scanning protocol was identical to that described previously (*22*). Briefly, after a transmission scan, 1,100 MBq of $H_2{}^{15}O$ dissolved in 5 mL saline were injected intravenously, followed by a 40-mL saline flush at a rate of 4 mL/s (bolus injection). A dynamic scan was acquired for a duration of 10 min. Subsequently, blood-pool imaging was performed. During a 2-min period, subjects inhaled at least 2,000 MBq of $C^{15}O$ and a single frame was acquired for a duration of 6 min, starting 1 min after the end of inhalation to allow for equilibration in the blood pool. During the $C^{15}O$ scan, 3 venous blood samples were drawn from the intravenous line and radioactivity was counted in a sodium iodide well counter cross-calibrated against the scanner. Emission data were corrected for the physical decay of ^{15}O, dead time, scatter, randoms, and photon attenuation. Reconstruction of the $H_2{}^{15}O$ emission sinograms was performed using filtered backprojection (FBP) with a Hanning filter at 0.5 of the Nyquist frequency. Transmission and $C^{15}O$ sinograms were iteratively reconstructed using ordered-subset expectation maximization ([OSEM], CTI version 7.1.1; 2 iterations, 16 subsets). OSEM images underwent 5-mm full width at half maximum (FWHM) gaussian postsmoothing to obtain a transaxial spatial resolution of ~7-mm FWHM, equal to that of FBP images (*23*).

MRI. MRI was performed on a 1.5-T scanner (Sonata; Siemens), using a 4-element phased-array body radiofrequency receiver coil. All images were acquired with electrocardiogram gating and during repeated breath-holds of 10–15 s, depending on the heart rate. After localizing scouts, cine images were acquired using a segmented steady-state-free precession sequence in 3 long-axis views (2-, 3-, and 4-chamber view) and in multiple short-axis views with a slice distance of 10 mm, covering the whole LV from base to apex. Scan parameters were as follows: temporal resolution, 34 ms; repetition time (TR), 3.0 ms; echo time (TE), 1.5 ms; typical voxel size, $1.4 \times 1.8 \times 5$ mm^3.

Contrast-enhanced images were acquired 15–20 min after intravenous administration of 0.2 mmol/kg gadolinium-diethylenetriaminepentaacetic acid (Fig. 1A) in the same view used as cine CMR, using a 2D segmented inversion-recovery prepared gradient-echo sequence (TE, 4.4 ms; TR, 9.8 ms; inversion time, 250–300 ms; typical voxel size, $1.3 \times 1.6 \times 5$ mm^3).

Data Analysis

PET. Anatomic tissue fraction (ATF) images were generated according to the procedure described by Iida et al. (*20*) Briefly, blood-volume images were normalized to the radioactivity in blood as measured from the samples. The reconstructed transmission data were normalized on a pixel-by-pixel basis to the average pixel counts in a region of interest (ROI) in the left ventricular chamber of the transmission image. Quantitative images of the ATF (mL/mL) were calculated taking into account the differences between the densities of blood and tissue.

Transaxial ATF images of the LV were reoriented according to the anatomic axis of the heart and slices were displayed as short-axis slices (Fig. 1B). The same reslicing parameters were applied to the dynamic $H_2{}^{15}O$ images. ROIs were defined manually at the basal and midventricular level of the LV as previously described (*22*). Corresponding ROIs from a variable number of slices were grouped in each patient to generate 12 volumes of interest (6 basal and 6 midventricular). The inferior volumes of interest were excluded from analysis because of anticipated perfusable tissue fraction (PTF) spillover effects from the liver (*22*).

Additional ROIs were defined in the left atrium and right ventricular chamber. This set of ROIs was projected on the dynamic $H_2{}^{15}O$ images to generate image-derived input functions. Using the standard single-tissue compartment model together with these input functions, myocardial blood flow (MBF) (mL/min/mL of perfusable tissue) and PTF (mL/mL) were determined for all myocardial tissue time–activity curves. Corrections were made for spillover from both the LV and right ventricle (RV) using the method described by Hermansen et al. (*24*) Global PET parameters were calculated by grouping all volumes of interest. In addition, septal and lateral parameters were determined by grouping of the

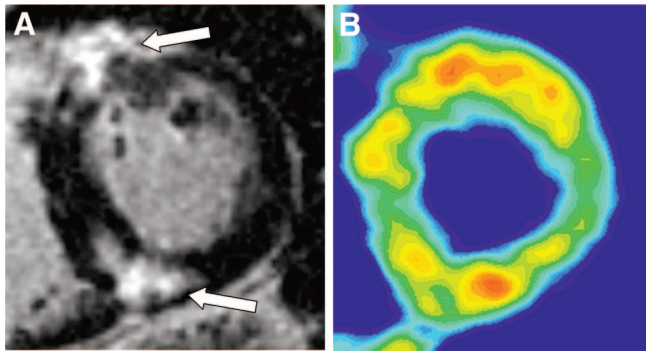

FIGURE 1. Midventricular short-axis view of a gadolinium delayed enhanced CMR image (A) of HCM patient. Note patchy hyperenhancement located at hypertrophied interventricular septum at junctions of septum and right ventricular free walls (arrows). (B) Anatomic tissue fraction image of same patient derived by PET.

TABLE 1
Characteristics of Control Subjects, HCM Patients, and MI Patients

Characteristic	Control (n = 6)	HCM (n = 21)	MI (n = 12)	P
Age (y)	50 ± 6	56 ± 12	58 ± 12	NS
Sex (M/F)	5/1	18/3	9/3	NS
NYHA functional class (I/II/III)	—	13/6/2	6/4/2	—
LVEF (%)	58 ± 4	65 ± 6	30 ± 11*	<0.01
IVS thickness (mm)	8 ± 1	21 ± 6†	7 ± 2	<0.01
LVPW thickness (mm)	6 ± 1	8 ± 2	6 ± 1	NS
Medication				
β-Blocker	—	8	11	—
Calcium antagonist	—	3	4	—

*P < 0.01 vs. control and HCM.
†P < 0.01 vs. control and MI.
NS = not significant; NYHA = New York Heart Association; LVEF = left ventricular ejection fraction; IVS = interventricular septum; LVPW = left ventricular posterior wall.

corresponding septal and lateral volumes of interest. As resting MBF is related to the rate–pressure product (RPP = heart rate × systolic blood pressure), corrected MBF (MBF/RPP × 10,000) was also determined. Finally, the PTI was obtained by dividing the PTF by the ATF.

MRI. The same regions on the short-axis slices were defined as described. Each myocardial segment was evaluated for the presence of hyperenhancement, defined as an area of signal enhancement > 2 SD of the signal of nonenhanced myocardium. The total myocardial area and the contrast-enhanced area per sector were traced manually. The extent of contrast enhancement was expressed as a percentage of the total myocardial area studied.

Statistical Analysis

Data are expressed as mean ± SD. For comparison of 2 datasets, paired or unpaired Student t tests were performed where appropriate. Comparison of multiple datasets was performed using ANOVA, and specific differences were identified by a Student t test corrected for multiple comparisons with the Bonferroni inequality adjustment. Correlations were analyzed using linear regression. A P value < 0.05 was considered significant.

RESULTS

Patient Population

Baseline characteristics are given in Table 1. The mean interventricular wall thickness was 21 ± 6 mm (range, 13–33 mm) in HCM patients.

DCE

CMR and PET data from healthy control subjects, HCM patients, and MI patients are summarized in Table 2. None of the control subjects demonstrated hyperenhancement. In 4 HCM patients (19%), virtually no hyperenhancement was present (<3% of myocardium). The mean DCE in HCM was 14% ± 12% (Fig. 2), predominantly localized at the junctions of the interventricular septum and the right ven-

TABLE 2
CMR and PET Data from Control Subjects, HCM Patients, and MI Patients

CMR and PET parameters	Control (n = 6)	HCM (n = 21)	MI (n = 12)	P
DCE (%)				
Average	—	14 ± 12	25 ± 16	<0.01
Septal	—	17 ± 15	29 ± 24	<0.05
Lateral	—	3 ± 2	22 ± 17	<0.05
MBF (mL/min/mL)				
Average	0.94 ± 0.22	0.88 ± 0.23	0.92 ± 0.27	NS
Septal	0.89 ± 0.27	0.82 ± 0.20	0.92 ± 0.32	NS
Lateral	0.99 ± 0.24	0.94 ± 0.31	0.91 ± 0.27	NS
PTI				
Average	1.10 ± 0.07	1.05 ± 0.12	0.94 ± 0.12*	<0.05
Septal	1.14 ± 0.05	1.12 ± 0.13	0.96 ± 0.21*	<0.05
Lateral	1.12 ± 0.12	1.03 ± 0.13†	0.93 ± 0.17*	<0.05

*P < 0.05 vs. control and HCM.
†P < 0.05 vs. control and MI.
NS = not significant.

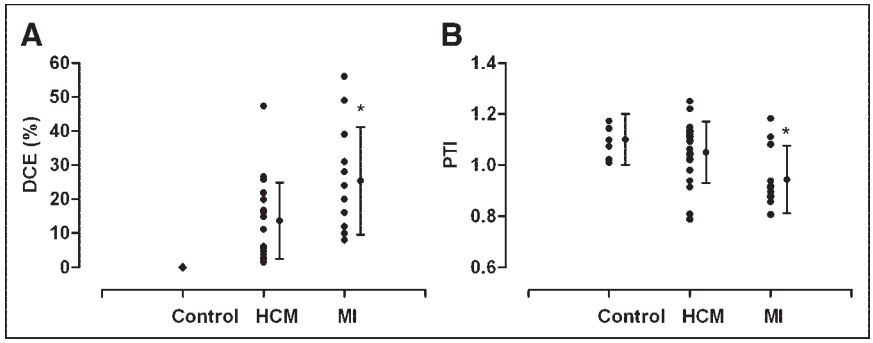

FIGURE 2. DCE (A) and PTI (B) for healthy control subjects, HCM patients, and MI patients. *$P < 0.05$ vs. control subjects and HCM patients.

tricular free wall (17% ± 15%), whereas virtually no DCE was observed in the lateral wall (3% ± 2%). All MI patients showed hyperenhancement with a mean value of 25% ± 16%, significantly higher compared with HCM patients.

MBF

In contrast to the control subjects, MBF was not homogeneously distributed in the HCM patients. Septal MBF was lower compared with the lateral wall (0.82 ± 0.20 vs. 0.94 ± 0.31 mL/min/mL; $P < 0.05$).

PTI

The PTI was reduced in the MI group compared with control subjects and HCM patients (Table 2; $P < 0.05$). The PTI did not differ between control subjects and HCM patients on a global level (Fig. 2), although the range was larger in HCM patients (0.79–1.25) than in control subjects (0.97–1.17). The PTI in the septum was comparable between control subjects and HCM patients. In HCM patients, however, the PTI in the lateral wall was reduced compared with that of the septum (1.03 ± 0.13 vs. 1.12 ± 0.13; $P < 0.01$). Furthermore, the PTI in the lateral wall was reduced compared with that of the control subjects (1.03 ± 0.13 vs. 1.12 ± 0.12; $P < 0.05$). As shown in Figure 3, segments without hyperenhancement had a lower PTI compared with hyperenhanced segments in HCM patients (1.02 ± 0.18 vs. 1.09 ± 0.19, respectively; $P < 0.05$).

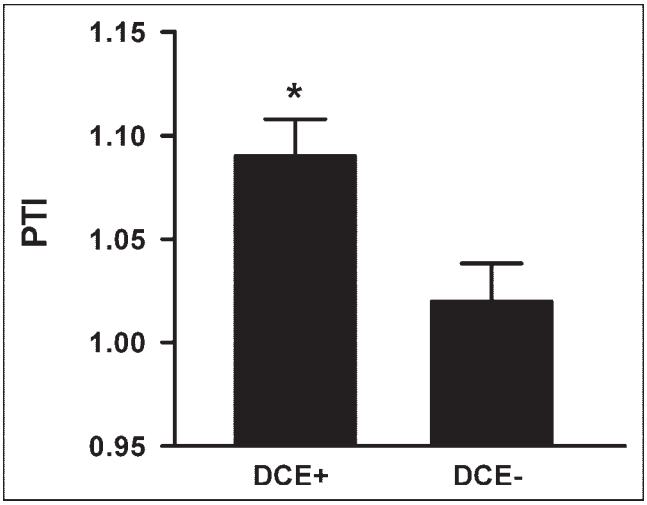

FIGURE 3. PTI for segments with (DCE+) and without (DCE−) hyperenhancement in HCM patients. PTI was significantly higher in areas with hyperenhancement. *$P < 0.05$ for DCE+ vs. DCE−.

Correlations Between CMR and PET Parameters

Global PTI correlated modestly with the extent of global DCE in HCM patients ($r = 0.45$, $P < 0.05$; Fig. 4). In MI patients, there was an inverse correlation between PTI and DCE ($r = -0.65$, $P < 0.05$). In addition, the left ventricular ejection fraction (LVEF) was inversely related to the extent of hyperenhancement ($r = -0.51$, $P < 0.05$) and the PTI ($r = -0.52$, $P < 0.05$; Fig. 5) in HCM patients. There was no correlation between maximum wall thickness and either DCE or PTI.

DISCUSSION

The similarity in distribution pattern between hyperenhanced areas visualized by DCE-CMR and scarring found in necropsy studies has led to the assumption that hyperenhancement in HCM represents fibrotic tissue (*16–18*). The present study was conducted to validate this hypothesis by comparing DCE-CMR with the PTI, an alternative validated marker of myocardial fibrosis (*19,21*).

Control Subjects

No hyperenhancement was observed in control subjects, and the PTI was in line with previous studies (*20,21*). For normal human myocardium, the PTF is approximately 10% higher than the ATF because venous blood volume of the heart is included in this parameter (~0.10 mL/g of net myocardium) (*25*). The expected value for the PTI in normal myocardium is therefore close to 1.1 (*20,21*).

Chronic MI

As might be expected, hyperenhancement was present in all patients with documented MI. In addition, the extent of hyperenhancement was directly related to the reduction in the PTI (Fig. 5), confirming the validity of both DCE-CMR and the PTI as noninvasive markers of scar tissue in chronic MI.

HCM

Hyperenhancement was observed in 81% of HCM patients, predominantly localized in the interventricular septum at the junctions of the septum and right ventricular free

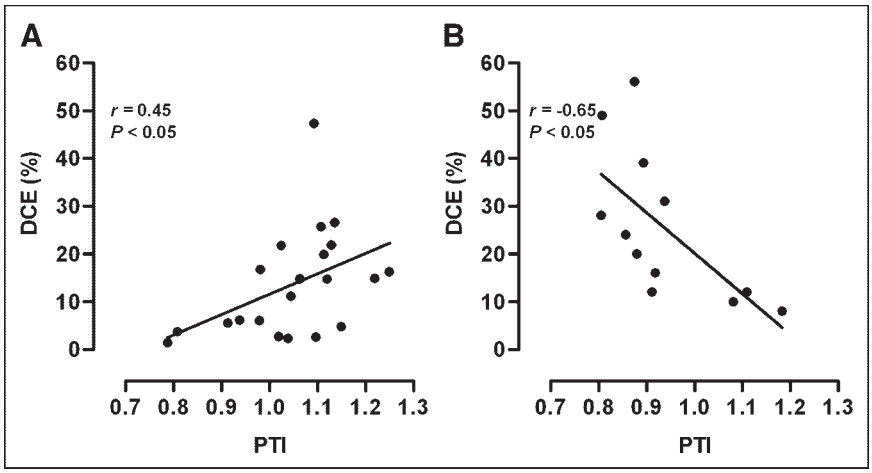

FIGURE 4. Scatter plots show relation between DCE and PTI in HCM patients (A) and MI patients (B).

wall. Furthermore, in line with Choudhury et al. (*17*), the extent of DCE was related to the LVEF (Fig. 5).

The PTI was reduced in the nonhypertrophied lateral free wall of HCM patients compared with that of control subjects. This can be explained by the presence of interstitial fibrosis, which is commonly found not only in the septum but also in the lateral wall, albeit to a lesser extent (*4,7,8,10*). Recently, a similar PTI reduction was found in patients with idiopathic dilated cardiomyopathy (*22*), a disease process also characterized by interstitial fibrosis. In addition, the observed absence of hyperenhancement in the lateral wall does not rule out the absence of fibrosis. As DCE depends on regional differences in gadolinium accumulation, it requires a reference area without hyperenhancement. In HCM, fibrosis is diffusely spread throughout the LV, lacking a normal reference area.

However, unlike our hypothesis, hyperenhancement in the hypertrophied interventricular septum of HCM patients was not accompanied by a decline in the PTI. Segments without hyperenhancement demonstrated lower PTI values than those with hyperenhancement (Fig. 3). Moreover, the extent of global hyperenhancement and the PTI were positively related, whereas, in the presence of myocardium and scar tissue alone, an inverse relation would be expected as found in patients with MI (Fig. 4).

Pathophysiologic Conditions in HCM and Its Relation to Hyperenhancement and PTI

The disease process of HCM is dynamic. Transgenic rodent models have demonstrated that histology is virtually normal in the early stages of the disorder, whereas, later in the disease process, myocardial disarray, hypertrophy, inflammation, myolysis, necrosis, and interstitial and replacement fibrosis can be observed (*26–28*). More advanced stages reveal increasing quantities of fibrotic tissue, whereas disarray and inflammation decrease. Furthermore, several types of fibrosis can be found in HCM patients (*6*), such as plexiform fibrosis. Formation of fibrosis in HCM may—next to primary connective tissue abnormalities—occur as a result of myocardial ischemia and infarction (*1,3,29*), causing the loss of cellular membrane integrity and interstitial edema. Human histopathology reports have shown similar results (*3,9,12,13*).

Gadolinium is an inert extracellular contrast agent, unable to cross the intact sarcolemmal membrane. Hyperenhancement of gadolinium is dependent on the volume of

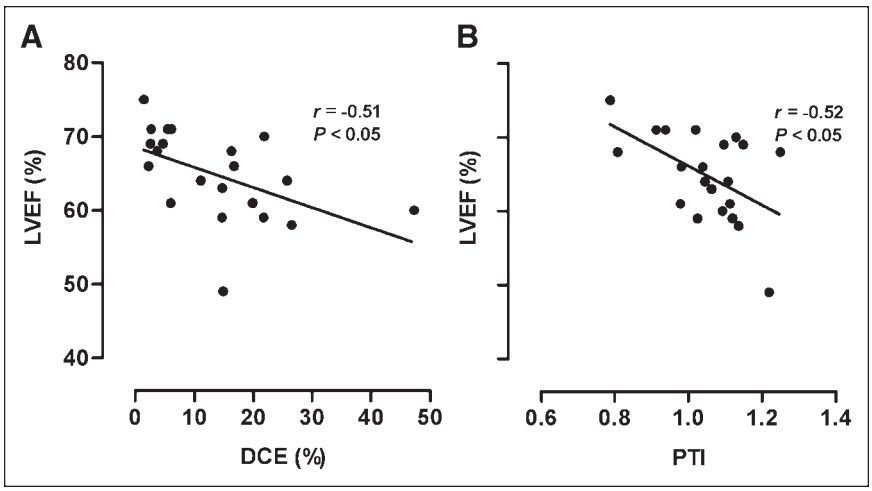

FIGURE 5. Scatter plots show relation between LVEF and DCE (A) and PTI (B) in HCM patients.

distribution (V_d) of the contrast agent and washin/washout kinetics (*30,31*). Hyperenhancement occurs not only in collagenous scar tissue but also in any condition accompanied by a larger V_d of gadolinium, such as disruption of cellular membrane, edema, and increased blood volume (*30,32,33*).

Therefore, hyperenhancement in HCM may be related not only to fibrosis but also to other conditions resulting in a larger V_d of gadolinium, such as disarray, inflammation, myolysis, and necrosis (*26–28*). This hypothesis is supported by an experimental study of Aso et al. (*28*), who found varying concentrations of gadolinium in transgenic HCM hamsters depending on the different stages of the disease process—that is, increased during the early stage of inflammation and lymphocytic infiltration as compared with less accumulation of gadolinium in the later stage characterized by more densely packed collagen fibers.

In the present study, hyperenhancement in the hypertrophied septum of HCM patients was characterized by a larger V_d of both gadolinium and water (Fig. 6), as PTI values were (near) normal in the septum of HCM patients. This is a distinctly different pattern than that observed in scar tissue of MI patients (i.e., increased V_d of gadolinium and decreased V_d of water-exchangeable tissue), suggesting a different histologic basis of hyperenhancement in HCM patients.

The PTI is the ratio of the PTF and the ATF. As the PTF is dependent on the V_d of water—that is, water-exchangeable tissue—the PTI is also dependent on the extent of water-exchangeable tissue. Because myocardial fibrosis is irrefutably present in the hypertrophied enhanced segments, a potential reduction of the PTI caused by fibrotic tissue, as observed in the lateral wall, could be compensated by an expansion of the water-diffusable volume surrounding the fibrotic tissue in the septum—the net result being a near-normal value for the PTI.

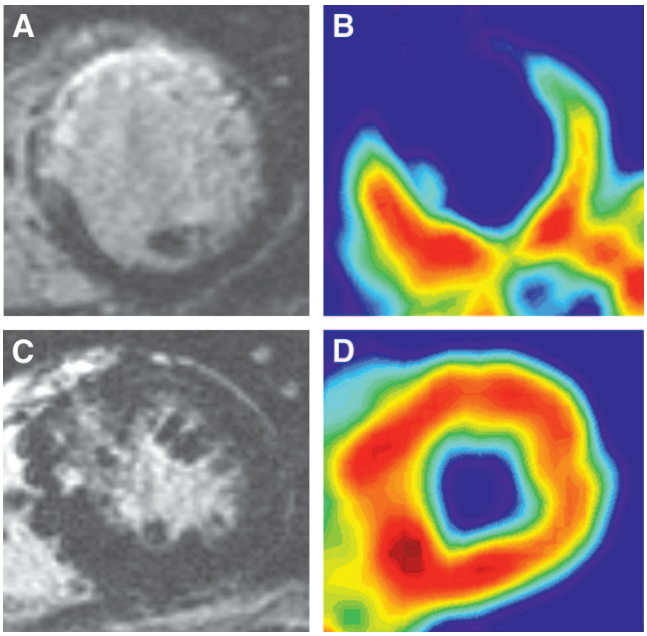

FIGURE 6. Short-axis view of DCE image (A) and parametric PTF image (B) in patient with anterior MI. Area of DCE matches absence of water-perfusable tissue in PTF image, indicating scar tissue. (C and D) Same images, as in A and B in HCM patient, demonstrate presence of water-perfusable tissue in hyperenhanced septal area.

As stated earlier, ischemia/necrosis and inflammation can be observed in HCM (*3,12,13,26–28*). Both conditions are accompanied by extravasation of fluid (edema), which is characterized by an increased water content of tissue. Interestingly, Inoue et al. observed a positive relation between water content and gadolinium accumulation in ischemic myocardium (*34*). Furthermore, during inflammation caused by myocarditis, transient hyperenhancement can be detected, which is related to the acute phase of lymphocytic infiltration and edema (*35,36*). Similar conditions in HCM could therefore be responsible for the presence of hyperenhancement in combination with water-diffusable tissue, explaining the preserved values of the PTI in the hyperenhanced myocardium.

Limitations

Corrections were made for both LV and RV spillover effects using a previously validated method (*24*). By definition, wall thickness of the interventricular septum is increased in patients with HCM, resulting in decreased spillover fractions from the LV and the RV and concomitant increased PTF and ATF values due to a reduction in the partial-volume effect. However, the PTI, being the ratio of the PTF and the ATF, will be virtually unaffected by these fluctuations in spillover and partial-volume effects as they affect the PTF and the ATF to a similar degree. Moreover, increasing wall thickness should result in more reliable data, as fewer corrections for spillover and partial-volume effects are made.

In addition, the spatial resolution of PET is considerably lower than that of CMR; therefore, it was not possible to accurately delineate regions that demonstrated DCE-CMR on the PET images. Instead, relative large, fixed anatomic sectors were used, which reflect a mixture of enhanced and nonenhanced tissue. One might argue that the PTI is not sensitive enough to detect the islands of fibrosis, explaining the similarity of the PTI values found in control subjects and HCM patients. This is, however, unlikely as the PTI was significantly reduced in the nonenhanced segments, suggestive of interstitial fibrosis. In the presence of scar tissue, the PTI in the enhanced segments would be expected to be even more reduced, whereas in those particular segments the PTI in HCM did not differ compared with that of control subjects. Nevertheless, histologic comparisons in patients with HCM are currently lacking and further studies on the use of the PTI as a marker of fibrosis are needed.

Furthermore, the extent and range of DCE was larger in MI patients than that in HCM patients, which might have resulted in a bias in the interpretation of the data. The latter limitation, however, cannot account for the observed oppo-

site correlation patterns between DCE and PTI in MI and HCM patients.

Finally, as the disease process of HCM is dynamic, it would be of special interest to perform serial matched DCE and PTI studies with relatively large time lags. Any alterations would provide more insight into the pathophysiologic basis of both DCE and PTI in HCM.

CONCLUSION

In asymmetric HCM patients, the PTI in the nonhypertrophied lateral wall is reduced, suggestive of the presence of interstitial fibrosis. However, in the hypertrophied interventricular septum, the PTI is not reduced and hyperenhancement by DCE-CMR can be observed. These results suggest that hyperenhancement in the hypertrophied septum is not solely caused by fibrotic replacement scarring. Other pathologic changes associated with HCM may also account for the hyperenhancement. Further studies are warranted with respect to the histologic basis of both DCE and PTI in HCM.

REFERENCES

1. Maron BJ. Hypertrophic cardiomyopathy: a systematic review. *JAMA.* 2002;287: 1308–1320.
2. Shirani J, Pick R, Roberts WC, Maron BJ. Morphology and significance of the left ventricular collagen network in young patients with hypertrophic cardiomyopathy and sudden cardiac death. *J Am Coll Cardiol.* 2000;35:36–44.
3. Basso C, Thiene G, Corrado D, Buja G, Melacini P, Nava A. Hypertrophic cardiomyopathy and sudden death in the young: pathologic evidence of myocardial ischemia. *Hum Pathol.* 2000;31:988–998.
4. Kuribayashi T, Roberts WC. Myocardial disarray at junction of ventricular septum and left and right ventricular free walls in hypertrophic cardiomyopathy. *Am J Cardiol.* 1992;70:1333–1340.
5. Yutani C, Imakita M, Ishibashi-Ueda H, et al. Three autopsy cases of progression to left ventricular dilatation in patients with hypertrophic cardiomyopathy. *Am Heart J.* 1985;109(3 Pt 1):545–553.
6. Anderson KR, Sutton MG, Lie JT. Histopathological types of cardiac fibrosis in myocardial disease. *J Pathol.* 1979;128:79–85.
7. Tanaka M, Fujiwara H, Onodera T, Wu DJ, Hamashima Y, Kawai C. Quantitative analysis of myocardial fibrosis in normals, hypertensive hearts, and hypertrophic cardiomyopathy. *Br Heart J.* 1986;55:575–581.
8. Unverferth DV, Baker PB, Pearce LI, Lautman J, Roberts WC. Regional myocyte hypertrophy and increased interstitial myocardial fibrosis in hypertrophic cardiomyopathy. *Am J Cardiol.* 1987;59:932–936.
9. Iida K, Yutani C, Imakita M, Ishibashi-Ueda H. Comparison of percentage area of myocardial fibrosis and disarray in patients with classical form and dilated phase of hypertrophic cardiomyopathy. *J Cardiol.* 1998;32:173–180.
10. Varnava AM, Elliott PM, Sharma S, McKenna WJ, Davies MJ. Hypertrophic cardiomyopathy: the interrelation of disarray, fibrosis, and small vessel disease. *Heart.* 2000;84:476–482.
11. Varnava AM, Elliott PM, Mahon N, Davies MJ, McKenna WJ. Relation between myocyte disarray and outcome in hypertrophic cardiomyopathy. *Am J Cardiol.* 2001;88:275–279.
12. Lamke GT, Allen RD, Edwards WD, Tazelaar HD, Danielson GK. Surgical pathology of subaortic septal myectomy associated with hypertrophic cardiomyopathy: a study of 204 cases (1996–2000). *Cardiovasc Pathol.* 2003;12:149–158.
13. Tazelaar HD, Billingham ME. The surgical pathology of hypertrophic cardiomyopathy. *Arch Pathol Lab Med.* 1987;111:257–260.
14. Wu E, Judd RM, Vargas JD, Klocke FJ, Bonow RO, Kim RJ. Visualisation of presence, location, and transmural extent of healed Q-wave and non-Q-wave myocardial infarction. *Lancet.* 2001;357:21–28.
15. Wagner A, Mahrholdt H, Holly TA, et al. Contrast-enhanced MRI and routine single photon emission computed tomography (SPECT) perfusion imaging for detection of subendocardial myocardial infarcts: an imaging study. *Lancet.* 2003; 361:374–379.
16. Moon JC, McKenna WJ, McCrohon JA, Elliott PM, Smith GC, Pennell DJ. Toward clinical risk assessment in hypertrophic cardiomyopathy with gadolinium cardiovascular magnetic resonance. *J Am Coll Cardiol.* 2003;41:1561–1567.
17. Choudhury L, Mahrholdt H, Wagner A, et al. Myocardial scarring in asymptomatic or mildly symptomatic patients with hypertrophic cardiomyopathy. *J Am Coll Cardiol.* 2002;40:2156–2164.
18. Moon JCC, Reed E, Sheppard MN, et al. The histologic basis of late gadolinium enhancement cardiovascular magnetic resonance in hypertrophic cardiomyopathy. *J Am Coll Cardiol.* 2004;43:2260–2264.
19. Iida H, Tamura Y, Kitamura K, Bloomfield PM, Eberl S, Ono Y. Histochemical correlates of ^{15}O-water-perfusable tissue fraction in experimental canine studies of old myocardial infarction. *J Nucl Med.* 2000;41:1737–1745.
20. Iida H, Rhodes CG, de Silva R, et al. Myocardial tissue fraction: correction for partial volume effects and measure of tissue viability. *J Nucl Med.* 1991;32: 2169–2175.
21. Knaapen P, Boellaard R, Gotte MJ, et al. The perfusable tissue index: a marker of myocardial viability. *J Nucl Cardiol.* 2003;10:684–691.
22. Knaapen P, Boellaard R, Gotte MJ, et al. Perfusable tissue index as a potential marker of fibrosis in patients with idiopathic dilated cardiomyopathy. *J Nucl Med.* 2004;45:1299–1304.
23. Boellaard R, van Lingen A, Lammertsma AA. Experimental and clinical evaluation of iterative reconstruction (OSEM) in dynamic PET: quantitative characteristics and effects on kinetic modeling. *J Nucl Med.* 2001;42:808–817.
24. Hermansen F, Rosen SD, Fath-Ordoubadi F, et al. Measurement of myocardial blood flow with oxygen-15 labelled water: comparison of different administration protocols. *Eur J Nucl Med.* 1998;25:751–759.
25. Crystal GJ, Downey HF, Bashour FA. Small vessel and total coronary blood volume during intracoronary adenosine. *Am J Physiol.* 1981;241:H194–H201.
26. Geisterfer-Lowrance AA, Christe M, Conner DA, et al. A mouse model of familial hypertrophic cardiomyopathy. *Science.* 1996;272:731–734.
27. Tardiff JC, Factor SM, Tompkins BD, et al. A truncated cardiac troponin T molecule in transgenic mice suggests multiple cellular mechanisms for familial hypertrophic cardiomyopathy. *J Clin Invest.* 1998;101:2800–2811.
28. Aso H, Takeda K, Ito T, Shiraishi T, Matsumura K, Nakagawa T. Assessment of myocardial fibrosis in cardiomyopathic hamsters with gadolinium-DTPA enhanced magnetic resonance imaging. *Invest Radiol.* 1998;33:22–32.
29. Cecchi F, Olivotto I, Gistri R, Lorenzoni R, Chiriatti G, Camici PG. Coronary microvascular dysfunction and prognosis in hypertrophic cardiomyopathy. *N Engl J Med.* 2003;349:1027–1035.
30. Kim RJ, Chen EL, Lima JA, Judd RM. Myocardial Gd-DTPA kinetics determine MRI contrast enhancement and reflect the extent and severity of myocardial injury after acute reperfused infarction. *Circulation.* 1996;94:3318–3326.
31. Kim RJ, Fieno DS, Parrish TB, et al. Relationship of MRI delayed contrast enhancement to irreversible injury, infarct age, and contractile function. *Circulation.* 1999;100:1992–2002.
32. Saeed M, Lund G, Wendland MF, Bremerich J, Weinmann H, Higgins CB. Magnetic resonance characterization of the peri-infarction zone of reperfused myocardial infarction with necrosis-specific and extracellular nonspecific contrast media. *Circulation.* 2001;103:871–876.
33. Abdel-Aty H, Zagrosek A, Schulz-Menger J, et al. Delayed enhancement and T2-weighted cardiovascular magnetic resonance imaging differentiate acute from chronic myocardial infarction. *Circulation.* 2004;109:2411–2416.
34. Inoue S, Murakami Y, Ochiai K, et al. The contributory role of interstitial water in Gd-DTPA-enhanced MRI in myocardial infarction. *J Magn Reson Imaging.* 1999;9:215–219.
35. Friedrich MG, Strohm O, Schulz-Menger J, Marciniak H, Luft FC, Dietz R. Contrast media-enhanced magnetic resonance imaging visualizes myocardial changes in the course of viral myocarditis. *Circulation.* 1998;97:1802–1809.
36. Mahrholdt H, Goedecke C, Wagner A, et al. Cardiovascular magnetic resonance assessment of human myocarditis: a comparison to histology and molecular pathology. *Circulation.* 2004;109:1250–1258.